

# A Study of Human Gaze Behavior During Visual Crowd Counting

Raji Annadi<sup>1</sup>, Yupei Chen<sup>2</sup>, Viresh Ranjan<sup>1</sup>,  
Dimitris Samaras<sup>1</sup>, Gregory Zelinsky<sup>2</sup>, Minh Hoai<sup>1</sup>

<sup>1</sup>Department of Computer Science, <sup>2</sup>Department of Psychology  
Stony Brook University, Stony Brook, NY 11790

## Abstract

In this paper, we describe our study on how humans allocate their attention during visual crowd counting. Using an eye tracker, we collect gaze behavior of human participants who are tasked with counting the number of people in crowd images. Analyzing the collected gaze behavior of ten human participants on thirty crowd images, we observe some common approaches for visual counting. For an image of a small crowd, the approach is to enumerate over all people or groups of people in the crowd, and this explains the high level of similarity between the fixation density maps of different human participants. For an image of a large crowd, our participants tend to focus on one section of the image, count the number of people in that section, and then extrapolate to the other sections. In terms of count accuracy, our human participants are not as good at the counting task, compared to the performance of the current state-of-the-art computer algorithms. Interestingly, there is a tendency to under count the number of people in all crowd images. Gaze behavior data and images can be downloaded from [https://www3.cs.stonybrook.edu/~minhhoai/projects/crowd\\_counting\\_gaze/](https://www3.cs.stonybrook.edu/~minhhoai/projects/crowd_counting_gaze/).

## 1 Introduction

Large crowd gathering is commonplace, and estimating the size of a crowd is an important problem for different purposes ranging from journalism to public safety. It is known that humans are good at subitizing [6], i.e., predicting fast and accurate counts for small number of items. For an image of a dense crowd, humans can also provide a very accurate count given enough time. In fact, one common approach to produce ‘gold standard’ annotations [3, 4, 22, 27] for training computer algorithms [1, 2, 4, 5, 7–21, 23–26, 28] for crowd counting is to ask human annotators to enumerate and place a dot on each person in the crowd images. The things that remain unclear are: 1) how well can humans count a large number of objects in dense images under limited time, and 2) what are the approaches that humans typically use for counting when there is not enough time to attend to and enumerate over all objects. In this paper, we seek the answers to these two questions by collecting and analyzing the gaze behavior of human subjects that were asked to count under a time constraint.

## 2 Data Collection

The gaze-behavior dataset we collected consists of 23,036 fixations from 10 participants with the task of counting the number of people in 30 images for 30 seconds per image. The 10 participants were Stony Brook University undergraduate and graduate students (6 male, 4 female, age range 18–28, normal or corrected-to-normal vision). A total of 30 diverse images were selected from the UCF-QNRF dataset [4] and used in this data collection. These images contained as few as 65 people and as many as 12672 people and included both images taken in daylight and at night.

Each participant was instructed to freely view each image and count “how many people were there in the image?” Each trial started with a central fixation dot and the participant had to fixate at the dot and press a button to start the trial. When the image appeared, they had 30s to freely inspect the image and count

the number of people in that image. The image disappeared after 30 seconds and they were asked to type in a number that indicated the number of people in the image. The 30 images were randomly interleaved and it took  $\sim 20$  minutes to finish the experiment. Eye movements were recorded using an EyeLink 1000 eye-tracker in desktop configuration (SR research) with a sample rate at 1000Hz. Eye-tracker calibration was conducted at the beginning of the experiment. All participants completed the experiment in the same controlled laboratory condition.

### 3 Gaze Behavior Analysis

This section describes several notable patterns in the gaze behaviors of our ten participants, obtained by visualizing their fixation density maps. All fixation density maps of the 10 participants on 30 crowd images are shown in the last 30 figures of this paper.

Our first observation is that our participants use different approaches for images of sparse and dense crowds. For an image with a sparse crowd where the total number of people is small (less than approximately 100 people) such as the one in Figure 1a, the fixation density map covers the entire crowd area as can be seen in Figure 1b. This suggests that the participants pay attention to every area of the crowd, and they probably aim to account for every single person or group of people in the image. For an image with a denser crowd such as the one in Figure 2a, the fixation density map covers only a small part of the crowd. This is understandable given the size of the crowd and the impossibility of enumerating over all people in the crowd. For an image of a dense crowd, the fixation density maps reveal that our participants tend to focus on one section of the crowd, count or estimate the number of people in that section, and extrapolate to the other sections.

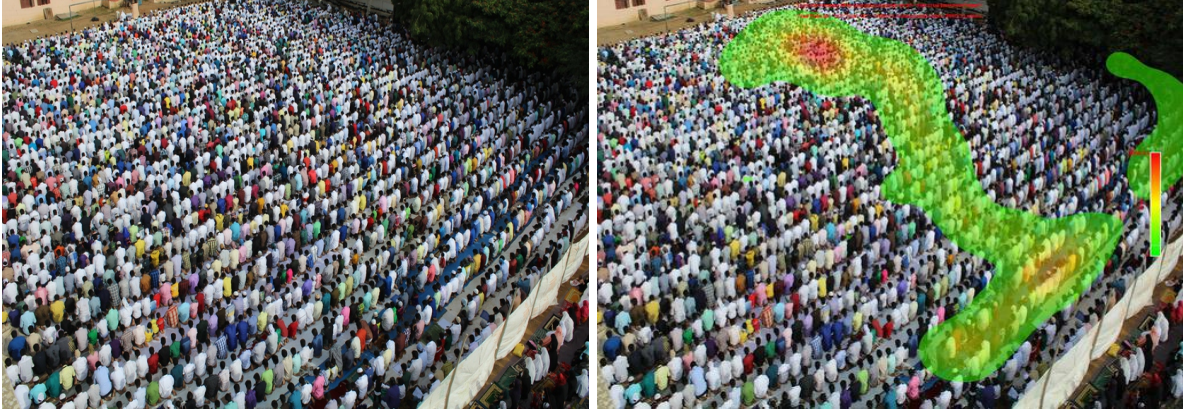


Figure 1: A sparse crowd image and the corresponding fixation density map

Our second observation is that the number of fixations tends to decrease as the size of the crowd increases, as can be seen in Figure 3. For a sparse crowd, our participants were fast to change their eye fixations, and this indicates an enumeration behavior. Meanwhile for a dense crowd, there is some region of the image where our participants attended to for a longer period of time to estimate the total count in the region.

Our third observation is that there is high degree of similarity between the fixation density maps of different subjects for an input image of a sparse crowd, as shown in Figure 4. This further indicates the behavior to account for all people or group of people in a sparse crowd.

We also find that our participants are more successful in estimating the size of a crowd with a uniform spread. Their common approach is to count the number of people in a selected row and selected column and multiple the resulting numbers to obtain the final count. This behavior can be observed in Figure 5, where each fixation density map spreads over one row and one column.



(a) A dense crowd image

(b) Fixation density map

Figure 2: A dense crowd image and the corresponding fixation density map

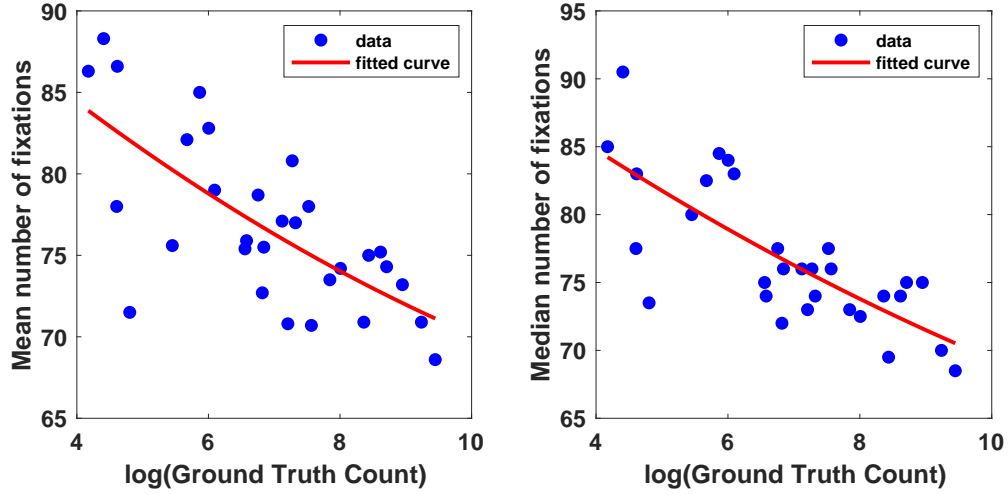


Figure 3: The mean and median number of fixations as a function of ground truth count. The number of fixations tends to decrease as the size of the crowd increases.

## 4 Count Accuracy

Table 1 lists the estimated counts from the 10 subjects on all 30 images. The images in the table are listed based on the sizes of the crowds, from smallest to largest. The table also reports the counting accuracy of the human subjects under several performance metrics. Following previous works on automated crowd counting (e.g., [1, 3, 4, 16, 27]), we evaluate the accuracy of human counting based on: Mean Absolute Error (MAE), Root Mean Squared Error (RMSE), Mean Normalized Absolute Error (MeanNAE), and Median Normalized Absolute Error (MedNAE). Let  $C_i$  denote the ground truth count for Image  $i$ , and  $\hat{C}_i^j$  is the estimated count





Figure 4: Fixation density maps of two different subjects on the same image with a sparse crowd. These density maps are highly similar to each other.



Figure 5: Fixation density maps from three different subjects on a crowd with a uniform density. The common behavior is to count the number of people in one row and count the number of rows.



	GT	Predicted counts of subjects										Mean	Median
	Count	Subj1	Subj2	Subj3	Subj4	Subj5	Subj6	Subj7	Subj8	Subj9	Subj10	NAE-I	NAE-I
Image 07	65	59	80	55	60	65	65	76	60	62	60	0.09	0.08
Image 08	82	90	70	90	45	55	40	65	50	62	90	0.26	0.23
Image 03	100	130	60	90	50	95	50	800	35	100	200	1.05	0.45
Image 06	101	68	80	110	60	160	50	150	60	65	170	0.40	0.41
Image 17	122	75	65	70	60	50	70	135	50	75	140	0.40	0.43
Image 09	233	230	100	110	180	300	150	320	120	120	220	0.34	0.36
Image 15	291	220	300	120	100	70	120	350	70	160	350	0.45	0.52
Image 10	353	350	250	175	200	350	180	350	150	200	500	0.32	0.42
Image 12	405	550	250	200	200	350	200	370	60	120	500	0.43	0.44
Image 22	443	250	350	200	400	300	400	500	200	150	500	0.32	0.27
Image 27	703	430	250	150	300	350	200	350	150	160	300	0.62	0.61
Image 14	720	350	600	250	400	5000	500	600	120	400	700	0.95	0.44
Image 30	858	700	200	225	350	250	300	400	150	130	600	0.61	0.68
Image 11	915	750	500	375	150	1000	400	10000	150	200	500	1.47	0.58
Image 02	936	580	400	300	500	3000	1500	5000	150	480	5000	1.49	0.64
Image 20	1237	800	1000	275	700	600	1800	1800	400	500	3500	0.63	0.49
Image 29	1349	2000	550	400	1000	5000	1200	1900	500	500	900	0.69	0.54
Image 05	1442	1600	2000	375	800	7000	1000	8000	100	400	4000	1.38	0.73
Image 01	1515	900	1000	350	1300	700	1000	800	500	900	1500	0.41	0.41
Image 28	1852	1400	500	350	800	17000	600	7000	600	250	4000	1.67	0.77
Image 13	1929	1200	600	500	600	14	1500	9000	100	500	20000	1.84	0.74
Image 23	2555	1300	1300	400	800	15500	1500	18000	300	1200	15000	2.03	0.77
Image 16	3002	2000	4000	600	3000	10000	1600	8000	700	1500	2000	0.75	0.48
Image 26	4282	1300	5000	650	1500	12000	2500	18000	800	1200	130000	3.87	0.77
Image 18	4609	4800	3000	700	2000	18000	1900	25000	700	3000	15000	1.32	0.72
Image 04	5520	3500	4000	1200	1000	10000	3000	15000	5000	1300	25000	0.96	0.77
Image 24	6052	2100	6000	700	5000	20000	3000	12400	1000	1000	12000	0.82	0.83
Image 25	7695	11000	10000	1400	1000	15000	5000	40000	2500	5000	28000	1.16	0.75
Image 21	10274	6500	6000	900	1500	12500	5000	80000	2000	4500	1000000	10.78	0.68
Image 19	12672	1600	1500	1200	4000	18000	9000	100000	2000	2500	1600000	13.79	0.86
MAE		1149	1050	1994	1475	3670	1025	9849	1785	1519	93453		
RMSE		2457	2327	3443	2836	5940	1650	22173	3081	2663	342365		
MeanNAE		0.34	0.39	0.64	0.49	1.54	0.43	2.42	0.68	0.55	9.63		
MedNAE		0.36	0.37	0.74	0.50	0.65	0.46	0.79	0.76	0.55	0.63		

Table 1: Ground truth and estimated counts from 10 different subjects on the 30 images. The images in the table are listed based on the sizes of the crowds. The table reports the Mean Absolute Error (MAE) and Root Mean Squared Error (RMSE) of individual subjects. This table also reports the Mean and Median Normalized Absolute Error (NAE) calculated for individual subjects (i.e., aggregating over images, referred as MeanNAE and MedNAE in the table) or individual images (i.e., aggregating over subjects, referred to as MeanNAE-I and MedNAE-I in the table).

from Subject  $j$  for Image  $i$ . The MAE, RMSE, MeanNAE and MedMAE for Subject  $j$  are defined as follows.

$$\text{MAE} = \frac{1}{n} \sum_{i=1}^n |C_i - \hat{C}_i^j|; \quad \text{RMSE} = \sqrt{\frac{1}{n} \sum_{i=1}^n (C_i - \hat{C}_i^j)^2}; \quad (1)$$

$$\text{MeanNAE} = \frac{1}{n} \sum_{i=1}^n \frac{|C_i - \hat{C}_i^j|}{C_i}; \quad \text{MedNAE} = \text{Median}_{i=1,n} \left\{ \frac{|C_i - \hat{C}_i^j|}{C_i} \right\}, \quad (2)$$

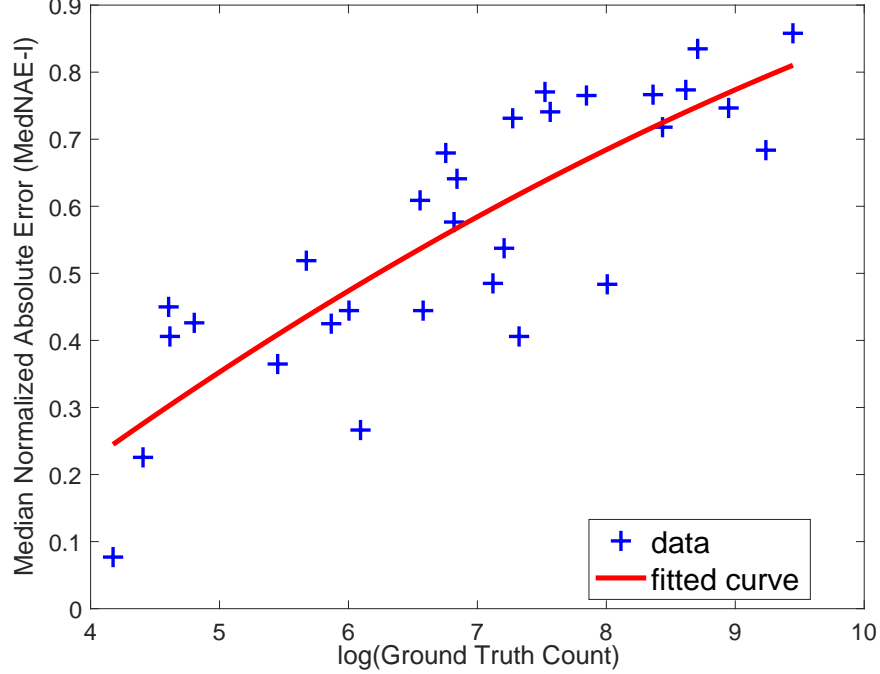


Figure 6: Median Normalized Absolute Error (MedNAE-I) versus the ground truth count in log scale. The MedNAE-I is somewhat linearly proportional to the logarithm of the crowd size.

where  $n = 30$  the number of images. We also compute the Mean NAE and Median NAE for each individual image by taking the mean or median over the 10 subjects. For Image  $i$ , the Mean NAE (MeanNAE-I) and Median NAE (MedNAE-I) are defined as follows:

$$\text{MeanNAE-I} = \frac{1}{m} \sum_{j=1}^m \frac{|C_i - \hat{C}_i^j|}{C_i}; \quad \text{MedNAE-I} = \text{Median}_{j=1, m} \left\{ \frac{|C_i - \hat{C}_i^j|}{C_i} \right\}, \quad (3)$$

where  $m = 10$  is the number of subjects.

As can be seen from Table 1, our human subjects are not as good at counting under time constraint, relative to the current state-of-the-art automated crowd counting methods. The lowest MAE and RMSE values are 1025 and 1650, respectively. As a reference, the MAE and RMSE of the DMCount method [21] on all test images of UCF-QNRF [4] are 85.6 and 148.3 respectively.

Comparing between images, we see that the absolute counting error is proportional to the size of crowd. However, the correlation between the absolute error and the crowd size is not linear. Considering the absolute error normalized by crowd size, the median value (MedNAE-I) is generally higher for a larger crowd, as can be seen from the last column of Table 1 and Figure 6.

Figure 7 is the scatter plot of the estimated counts and the ground truth counts. As can be seen, our human subjects tend to under-count the number of people in each image. On all images, the median and mean estimates are smaller than the ground truth. For images with smaller crowd sizes, the majority of the estimates are lower than the actual crowd sizes.

## 5 Conclusions

In this paper, we have presented a gaze-behavior dataset consisting of 23K fixations from 10 human participants on thirty crowd images. We have analyzed the gaze behavior of the human participants as well as the accuracy

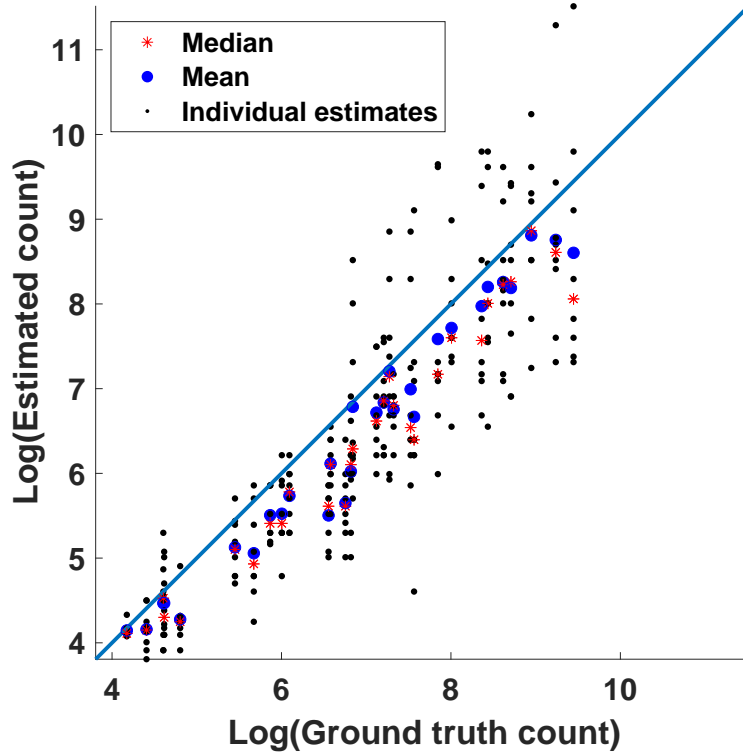


Figure 7: Estimated counts versus ground truth counts in log-scale plot. Black dots are the individual estimates from out subjects. For each image, the figure only shows eight out of ten estimates, removing the minimum and maximum estimated values; this corresponds to removing the possible outliers outside the 10 to 90 percentiles range. The blue circles and red stars are the mean and median values of the estimated values respectively. The estimates above the diagonal line correspond to over counting, while the ones below the diagonal line correspond to under counting. For all images, both mean and median values are lower than the actual counts. This indicates the under-counting tendency of our subjects. For images with a smaller number of people, most estimated counts are lower than the actual number of people in the image.



of their count estimates. We found that our human participants used different approaches for sparse and dense crowds, and the number of fixations tends to decrease as the size of the crowd increases. For a sparse crowd, the common approach of our participants was to enumerate over all people or group of people in the crowd, leading to fixation density maps that were highly similar to one another. For a denser crowd, our participants tended to focus on counting the number of people in a small section and then extrapolate to other sections. In terms of count accuracy, our human participants performed poorly, compared to the performance of the state-of-the-art computer algorithms. We also observed a tendency to under count the number of people in each image.

## References

- [1] X. Cao, Z. Wang, Y. Zhao, and F. Su. Scale aggregation network for accurate and efficient crowd counting. In *Proceedings of the European Conference on Computer Vision*, 2018.
- [2] Z.-Q. Cheng, J.-X. Li, Q. Dai, X. Wu, and A. G. Hauptmann. Learning spatial awareness to improve crowd counting. In *Proceedings of the International Conference on Computer Vision*, 2019.
- [3] H. Idrees, I. Saleemi, C. Seibert, and M. Shah. Multi-source multi-scale counting in extremely dense crowd images. In *Proceedings of the IEEE Conference on Computer Vision and Pattern Recognition*, 2013.
- [4] H. Idrees, M. Tayyab, K. Athrey, D. Zhang, S. Al-Maadeed, N. Rajpoot, and M. Shah. Composition loss for counting, density map estimation and localization in dense crowds. In *Proceedings of the European Conference on Computer Vision*, 2018.
- [5] X. Jiang, Z. Xiao, B. Zhang, X. Zhen, X. Cao, D. Doermann, and L. Shao. Crowd counting and density estimation by trellis encoder-decoder networks. In *Proceedings of the IEEE Conference on Computer Vision and Pattern Recognition*, 2019.
- [6] E. L. Kaufman, M. W. Lord, T. W. Reese, and J. Volkmann. The discrimination of visual number. *American Journal of Psychology*, 62:498–525, 1949.
- [7] Y. Li, X. Zhang, and D. Chen. Csrnet: Dilated convolutional neural networks for understanding the highly congested scenes. In *Proceedings of the IEEE Conference on Computer Vision and Pattern Recognition*, 2018.
- [8] D. Lian, J. Li, J. Zheng, W. Luo, and S. Gao. Density map regression guided detection network for rgb-d crowd counting and localization. In *Proceedings of the IEEE Conference on Computer Vision and Pattern Recognition*, 2019.
- [9] C. Liu, X. Weng, and Y. Mu. Recurrent attentive zooming for joint crowd counting and precise localization. In *Proceedings of the IEEE Conference on Computer Vision and Pattern Recognition*, 2019.
- [10] L. Liu, Z. Qiu, G. Li, S. Liu, W. Ouyang, and L. Lin. Crowd counting with deep structured scale integration network. In *Proceedings of the International Conference on Computer Vision*, 2019.
- [11] N. Liu, Y. Long, C. Zou, Q. Niu, L. Pan, and H. Wu. Adcrowdnet: An attention-injective deformable convolutional network for crowd understanding. In *Proceedings of the IEEE Conference on Computer Vision and Pattern Recognition*, 2019.
- [12] W. Liu, M. Salzmann, and P. Fua. Context-aware crowd counting. In *Proceedings of the IEEE Conference on Computer Vision and Pattern Recognition*, 2019.
- [13] Y. Liu, M. Shi, Q. Zhao, and X. Wang. Point in, box out: Beyond counting persons in crowds. In *Proceedings of the IEEE Conference on Computer Vision and Pattern Recognition*, 2019.
- [14] E. Lu, W. Xie, and A. Zisserman. Class-agnostic counting. In *Proceedings of the Asian Conference on Computer Vision*, 2018.
- [15] Z. Ma, X. Wei, X. Hong, and Y. Gong. Bayesian loss for crowd count estimation with point supervision. In *Proceedings of the International Conference on Computer Vision*, 2019.

- [16] V. Ranjan, H. Le, and M. Hoai. Iterative crowd counting. In *Proceedings of the European Conference on Computer Vision*, 2018.
- [17] V. Ranjan, B. Wang, M. Shah, and M. Hoai. Uncertainty estimation and sample selection for crowd counting. In *Proceedings of the Asian Conference on Computer Vision*, 2020.
- [18] M. Shi, Z. Yang, C. Xu, and Q. Chen. Revisiting perspective information for efficient crowd counting. In *Proceedings of the IEEE Conference on Computer Vision and Pattern Recognition*, 2019.
- [19] J. Wan and A. Chan. Adaptive density map generation for crowd counting. In *Proceedings of the International Conference on Computer Vision*, 2019.
- [20] J. Wan, W. Luo, B. Wu, A. B. Chan, and W. Liu. Residual regression with semantic prior for crowd counting. In *Proceedings of the IEEE Conference on Computer Vision and Pattern Recognition*, 2019.
- [21] B. Wang, H. Liu, D. Samaras, and M. Hoai. Distribution matching for crowd counting. In *Advances in Neural Information Processing Systems*, 2020.
- [22] Q. Wang, J. Gao, W. Lin, and X. Li. Nwpu-crowd: A large-scale benchmark for crowd counting. *arXiv preprint arXiv:2001.03360*, 2020.
- [23] Q. Wang, J. Gao, W. Lin, and Y. Yuan. Learning from synthetic data for crowd counting in the wild. In *Proceedings of the IEEE Conference on Computer Vision and Pattern Recognition*, 2019.
- [24] C. Xu, K. Qiu, J. Fu, S. Bai, Y. Xu, and X. Bai. Learn to scale: Generating multipolar normalized density maps for crowd counting. In *Proceedings of the International Conference on Computer Vision*, 2019.
- [25] Z. Yan, Y. Yuan, W. Zuo, X. Tan, Y. Wang, S. Wen, and E. Ding. Perspective-guided convolution networks for crowd counting. In *Proceedings of the International Conference on Computer Vision*, 2019.
- [26] Q. Zhang and A. B. Chan. Wide-area crowd counting via ground-plane density maps and multi-view fusion cnns. In *Proceedings of the IEEE Conference on Computer Vision and Pattern Recognition*, 2019.
- [27] Y. Zhang, D. Zhou, S. Chen, S. Gao, and Y. Ma. Single-image crowd counting via multi-column convolutional neural network. In *Proceedings of the IEEE Conference on Computer Vision and Pattern Recognition*, 2016.
- [28] M. Zhao, J. Zhang, C. Zhang, and W. Zhang. Leveraging heterogeneous auxiliary tasks to assist crowd counting. In *Proceedings of the IEEE Conference on Computer Vision and Pattern Recognition*, 2019.

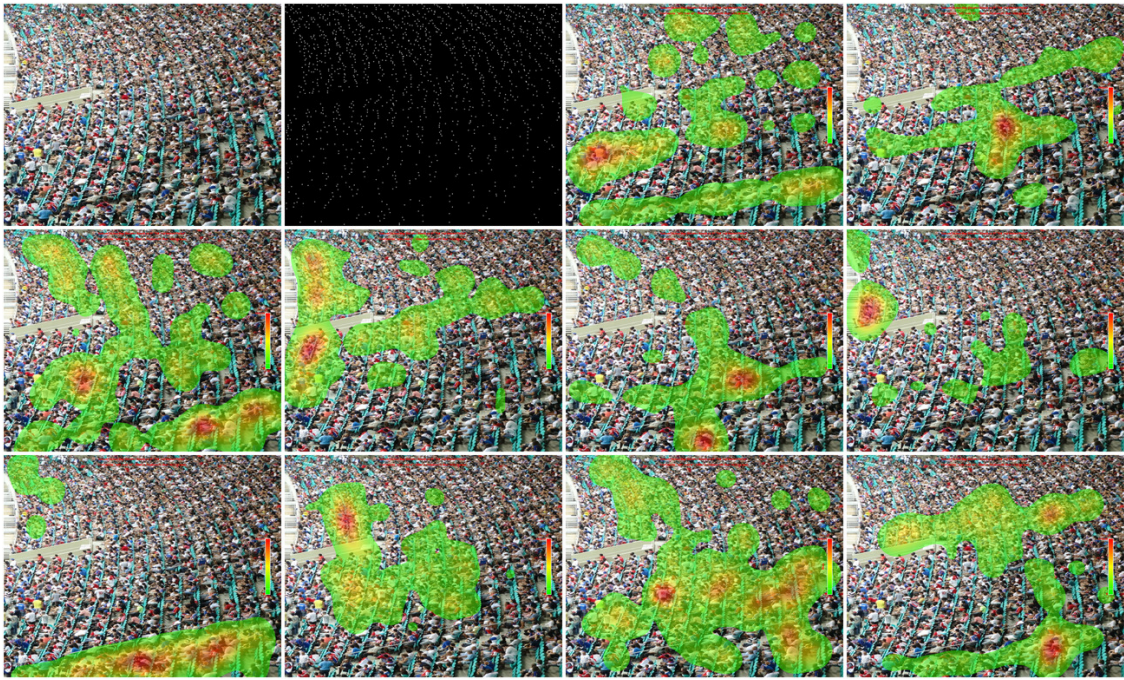


Figure 8: Image grid containing image 1, its annotation and fixation density maps from all subjects.

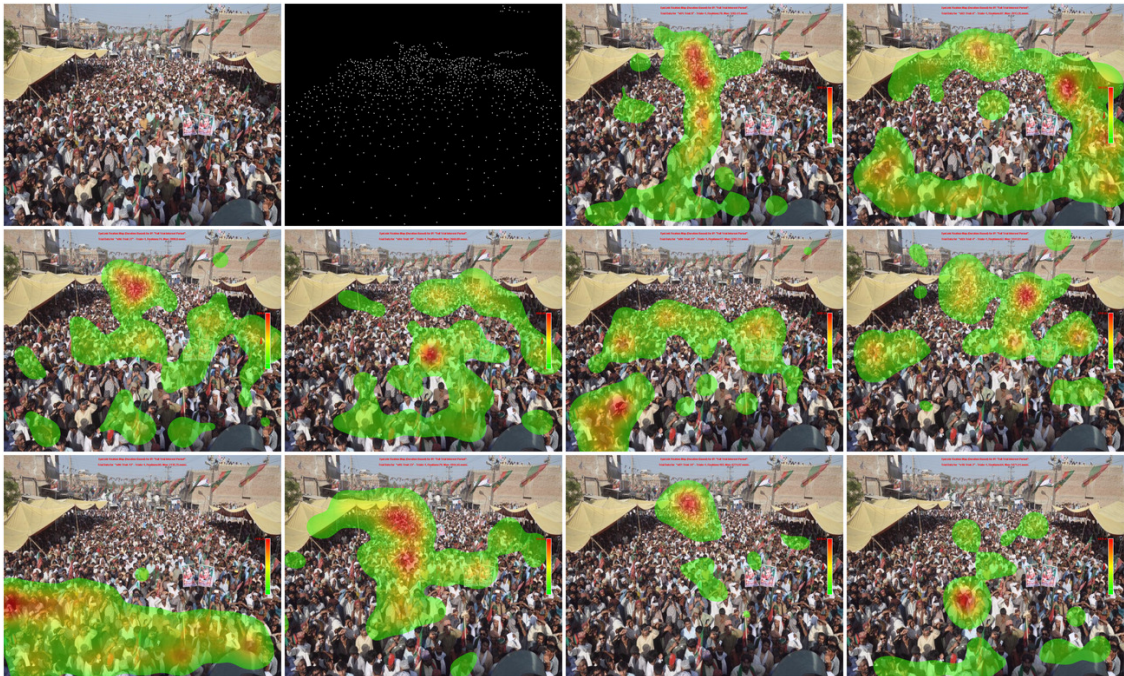


Figure 9: Image grid containing image 2, its annotation and fixation density maps from all subjects.



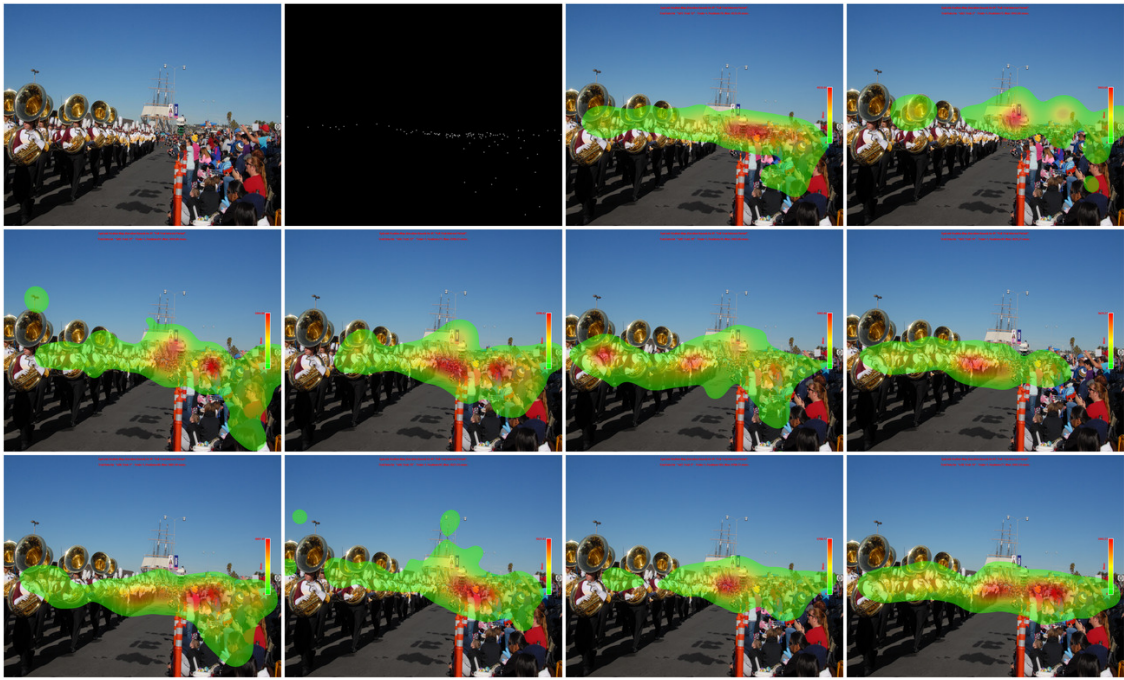


Figure 10: Image grid containing image 3, its annotation and fixation density maps from all subjects.

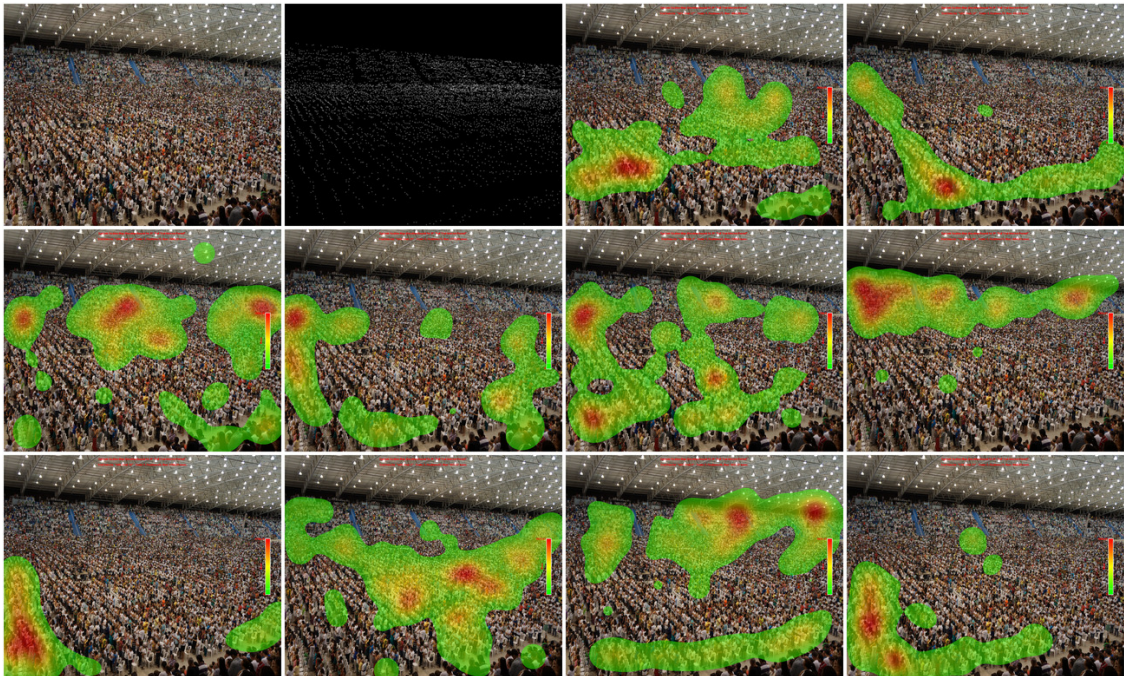


Figure 11: Image grid containing image 4, its annotation and fixation density maps from all subjects.



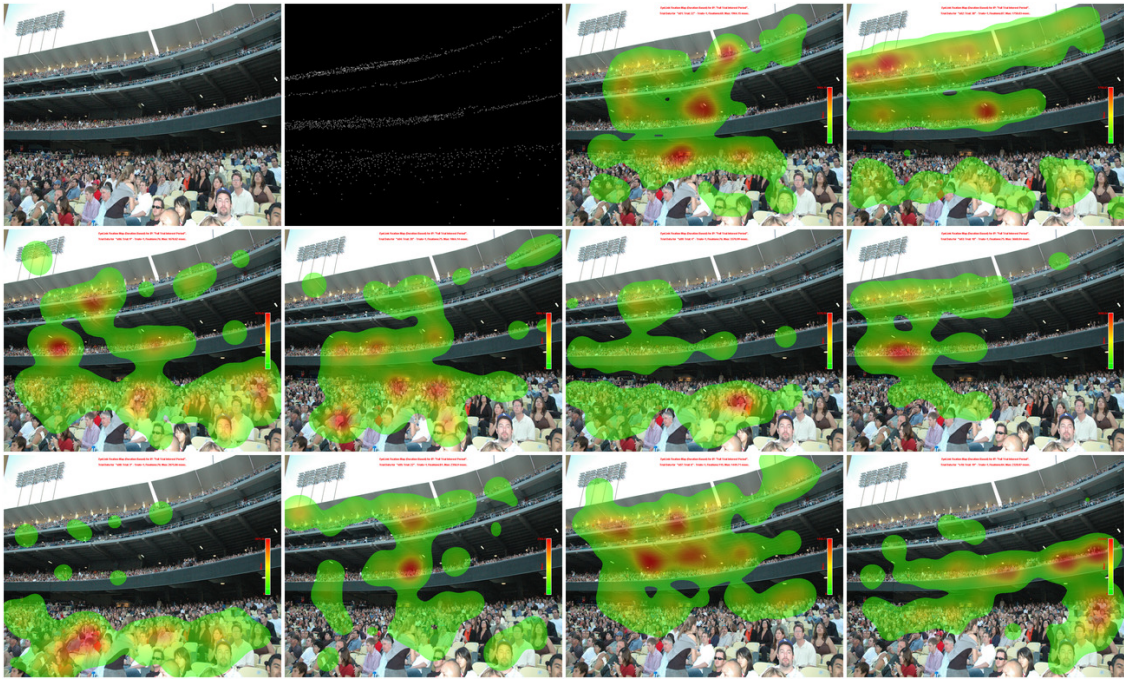


Figure 12: Image grid containing image 5, its annotation and fixation density maps from all subjects.

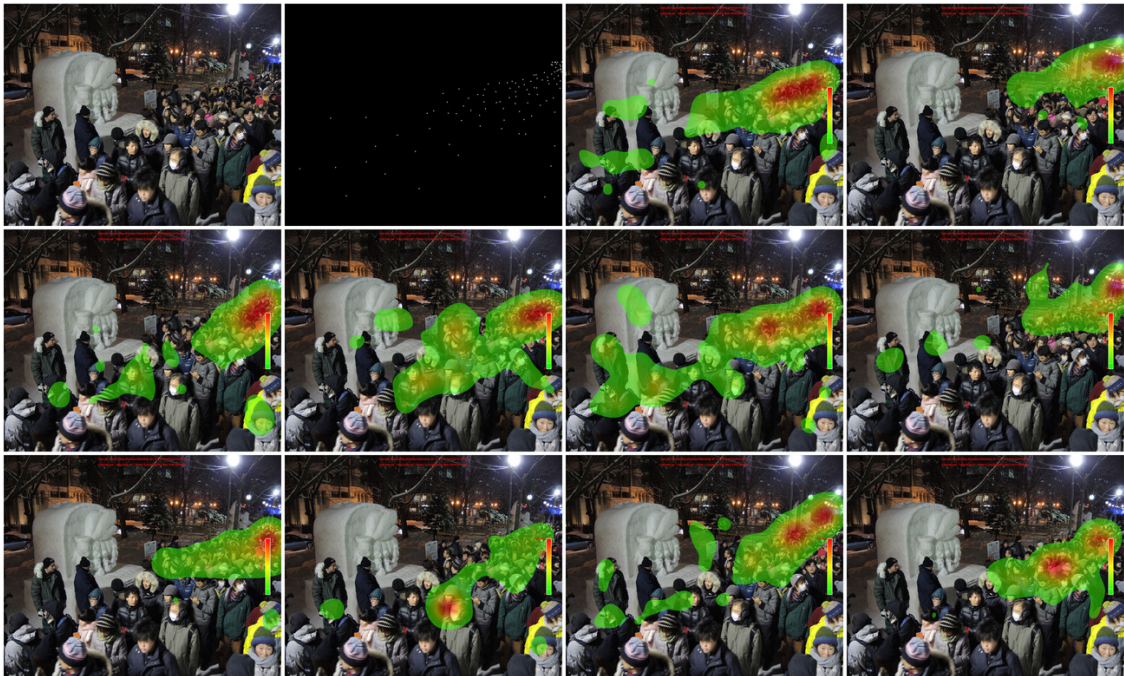


Figure 13: Image grid containing image 6, its annotation and fixation density maps from all subjects.





Figure 14: Image grid containing image 7, its annotation and fixation density maps from all subjects.

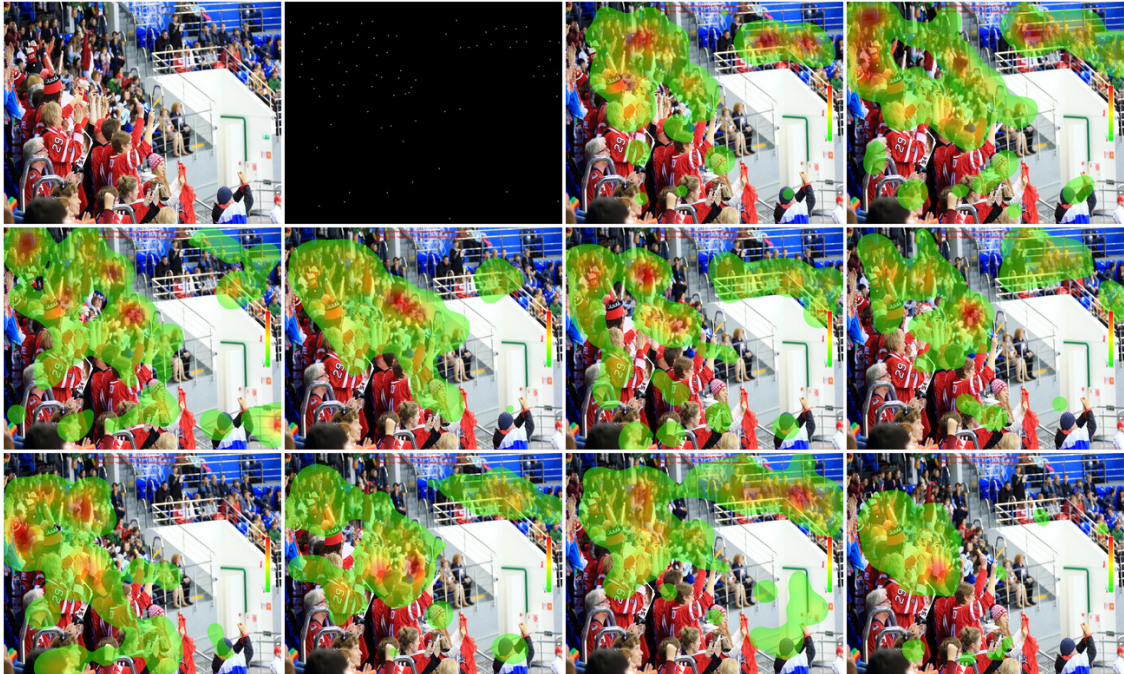


Figure 15: Image grid containing image 8, its annotation and fixation density maps from all subjects.





Figure 16: Image grid containing image 9, its annotation and fixation density maps from all subjects.

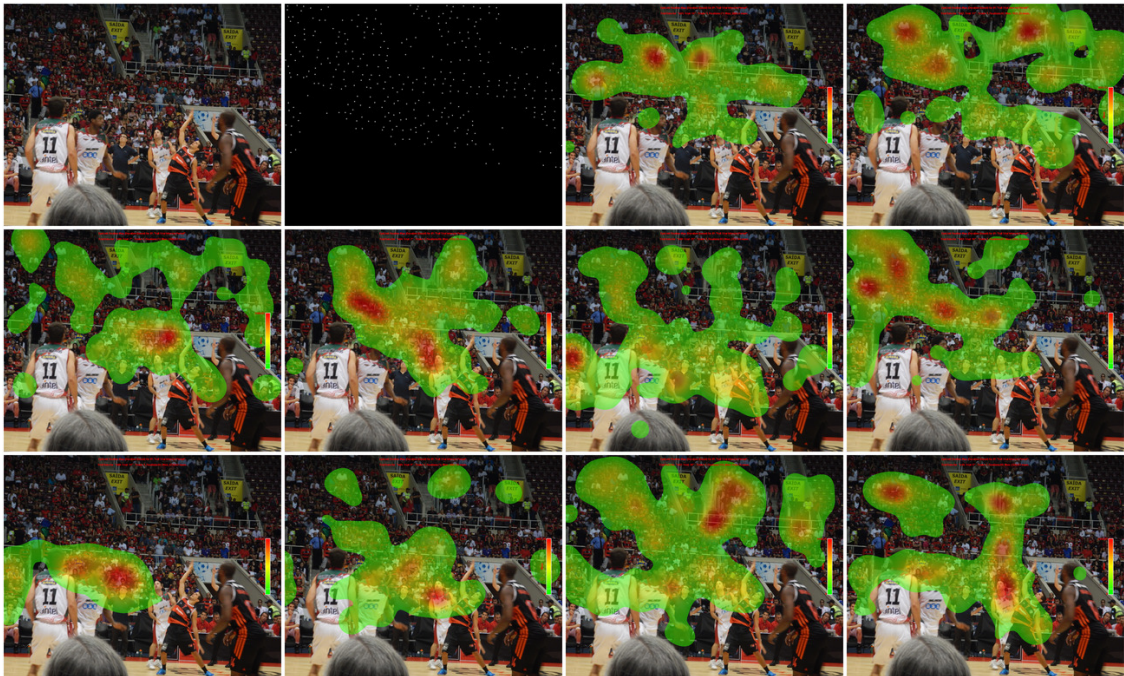


Figure 17: Image grid containing image 10, its annotation and fixation density maps from all subjects.



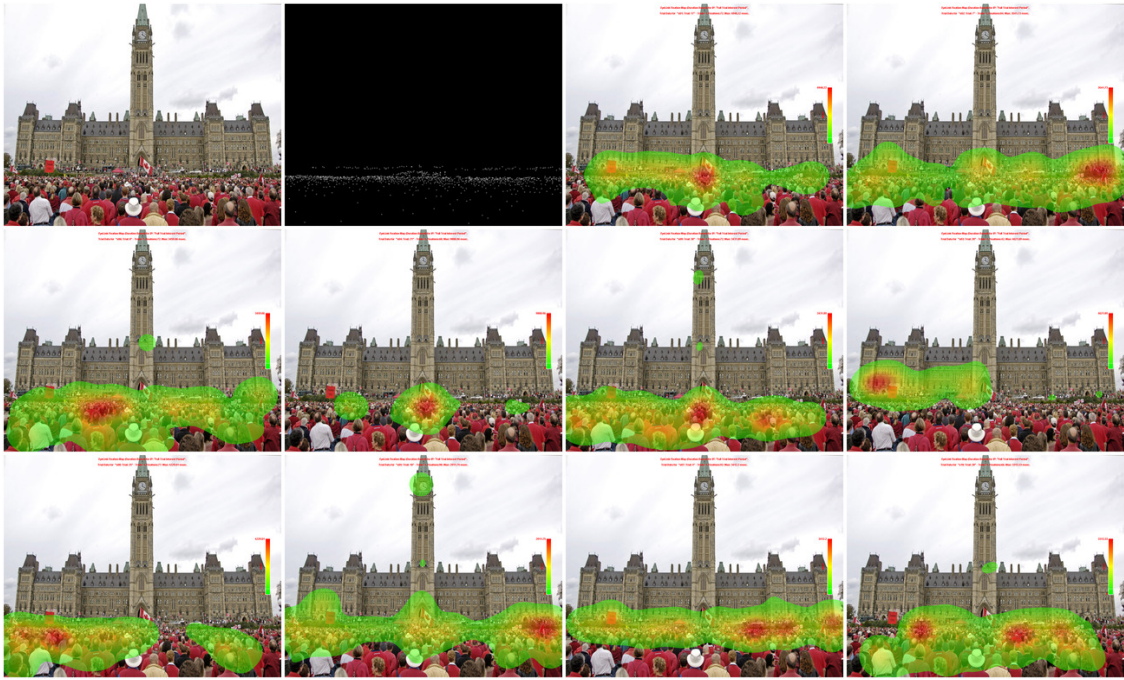


Figure 18: Image grid containing image 11, its annotation and fixation density maps from all subjects.

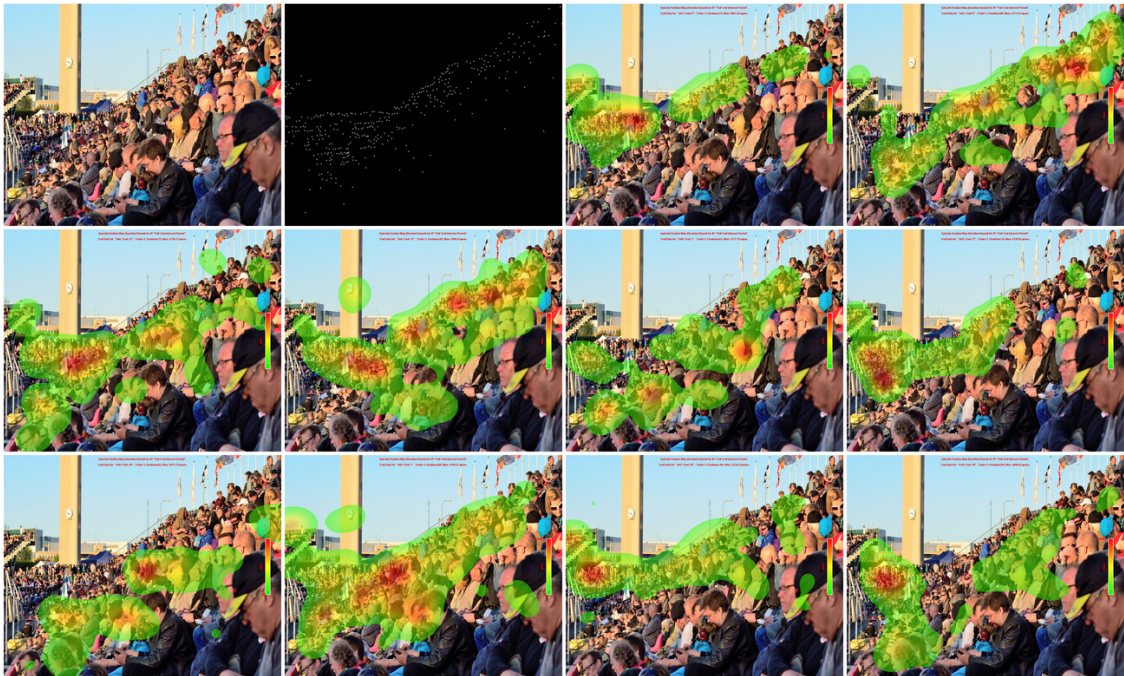


Figure 19: Image grid containing image 12, its annotation and fixation density maps from all subjects.



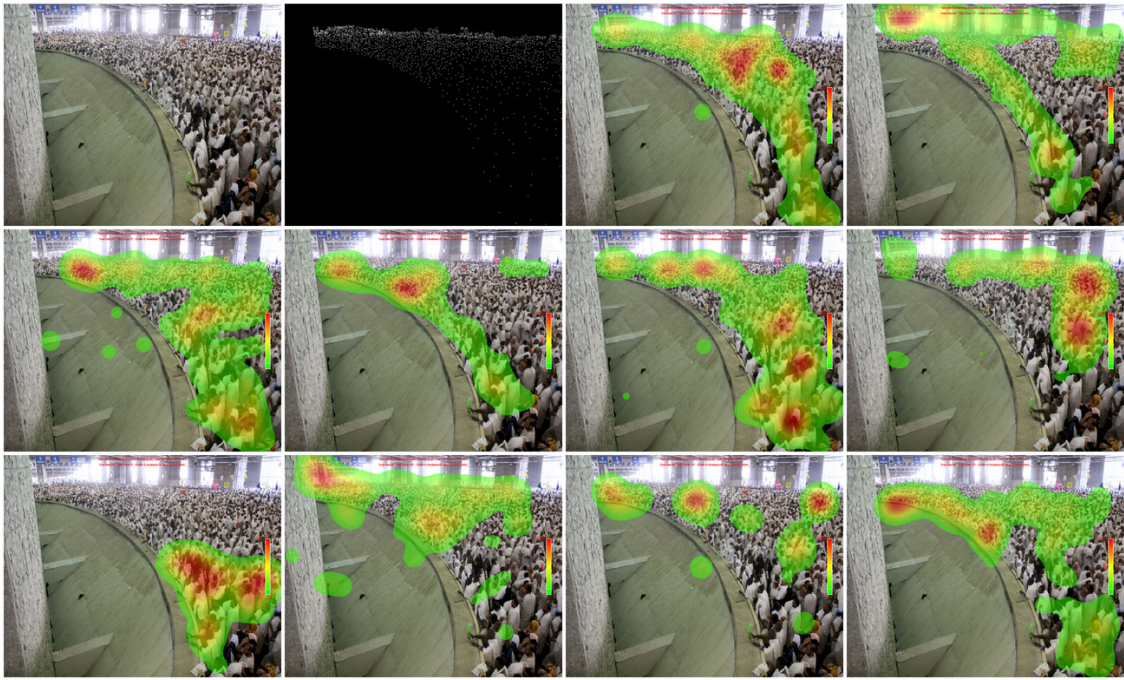


Figure 20: Image grid containing image 13, its annotation and fixation density maps from all subjects.

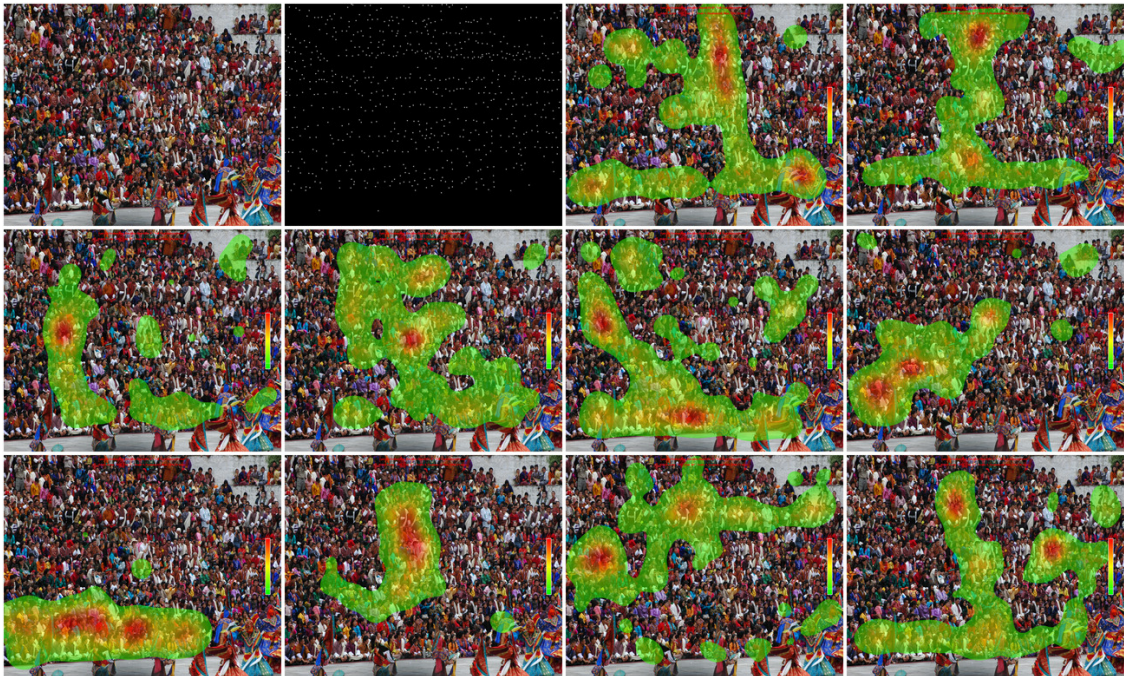


Figure 21: Image grid containing image 14, its annotation and fixation density maps from all subjects.



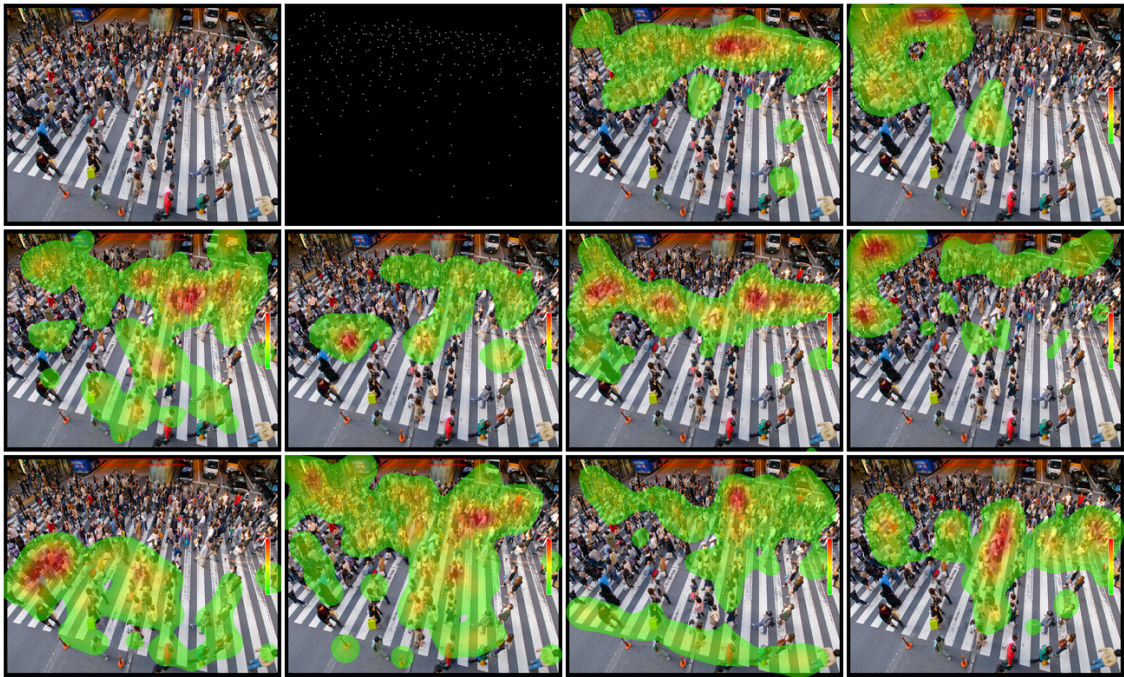


Figure 22: Image grid containing image 15, its annotation and fixation density maps from all subjects.

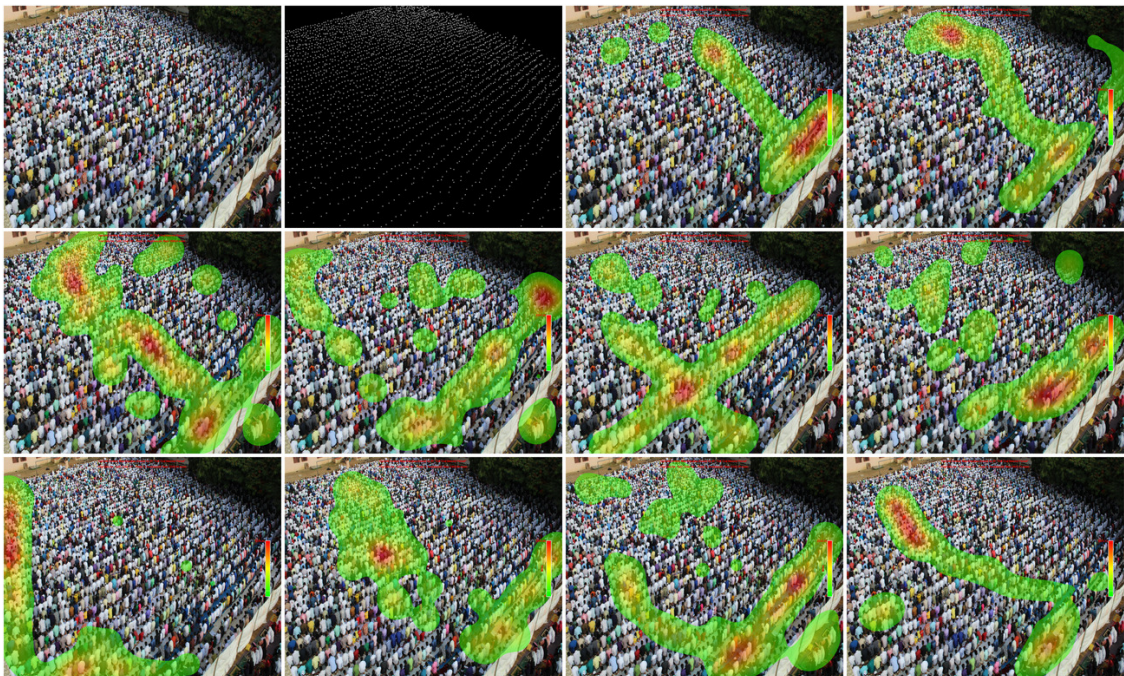


Figure 23: Image grid containing image 16, its annotation and fixation density maps from all subjects.



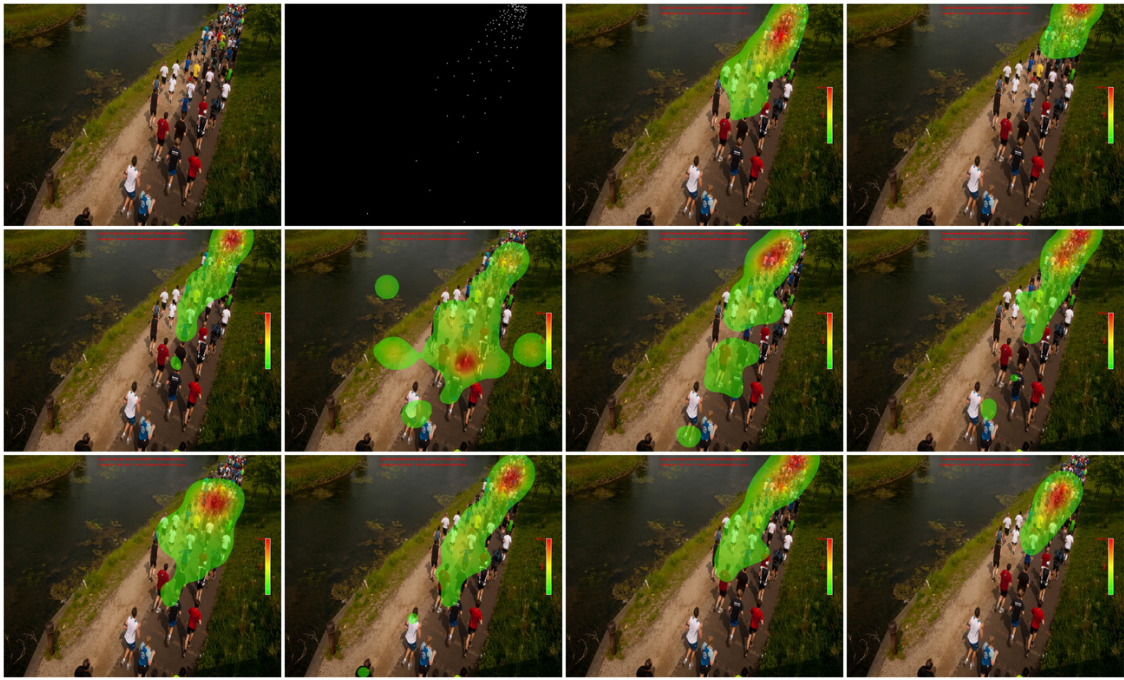


Figure 24: Image grid containing image 17, its annotation and fixation density maps from all subjects.

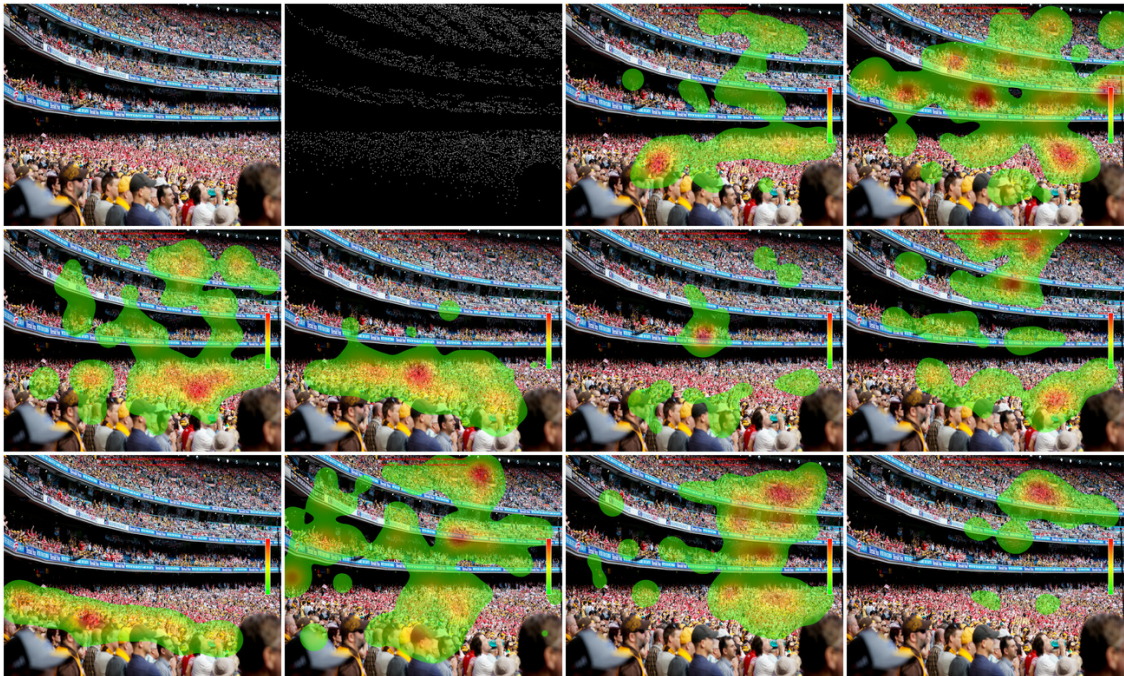


Figure 25: Image grid containing image 18, its annotation and fixation density maps from all subjects.



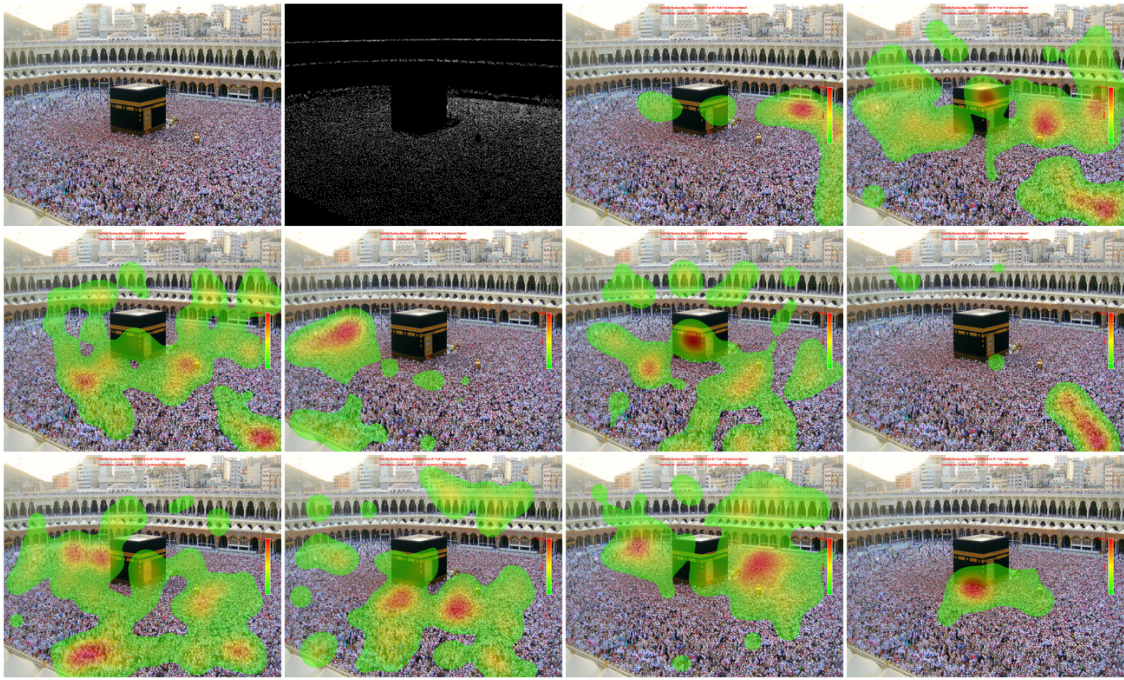


Figure 26: Image grid containing image 19, its annotation and fixation density maps from all subjects.

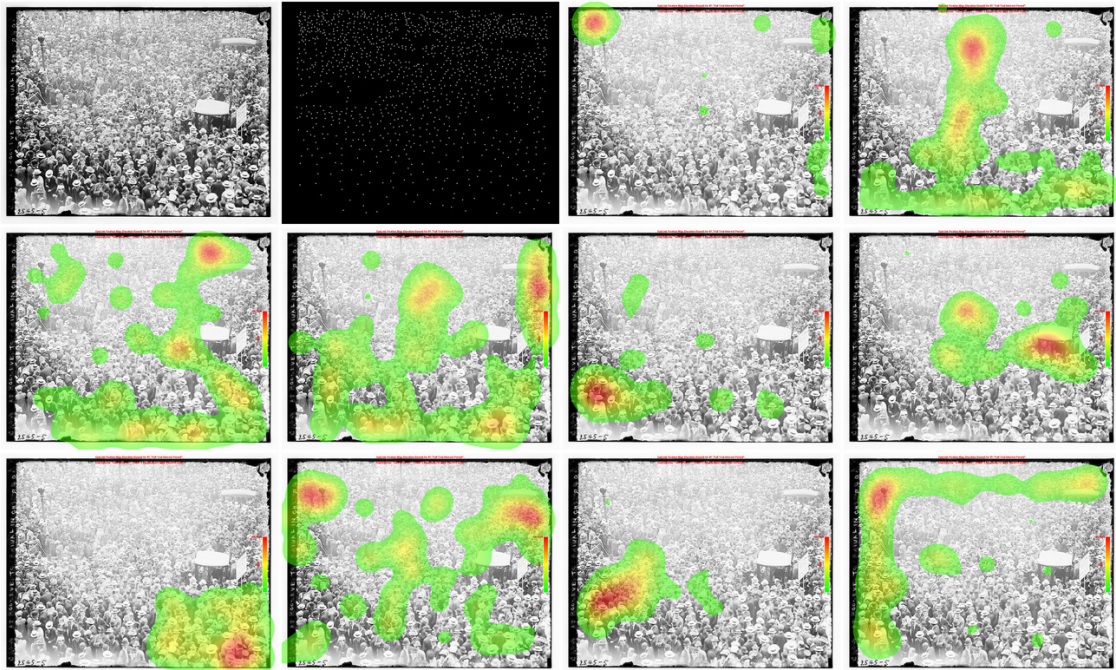


Figure 27: Image grid containing image 20, its annotation and fixation density maps from all subjects.



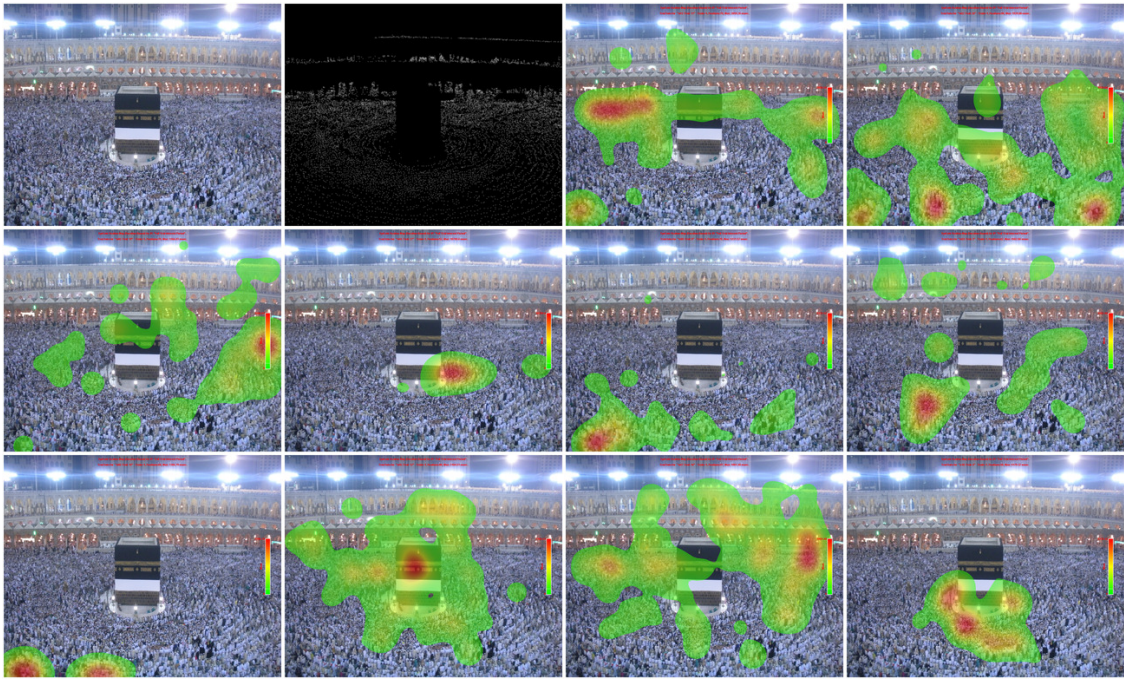


Figure 28: Image grid containing image 21, its annotation and fixation density maps from all subjects.

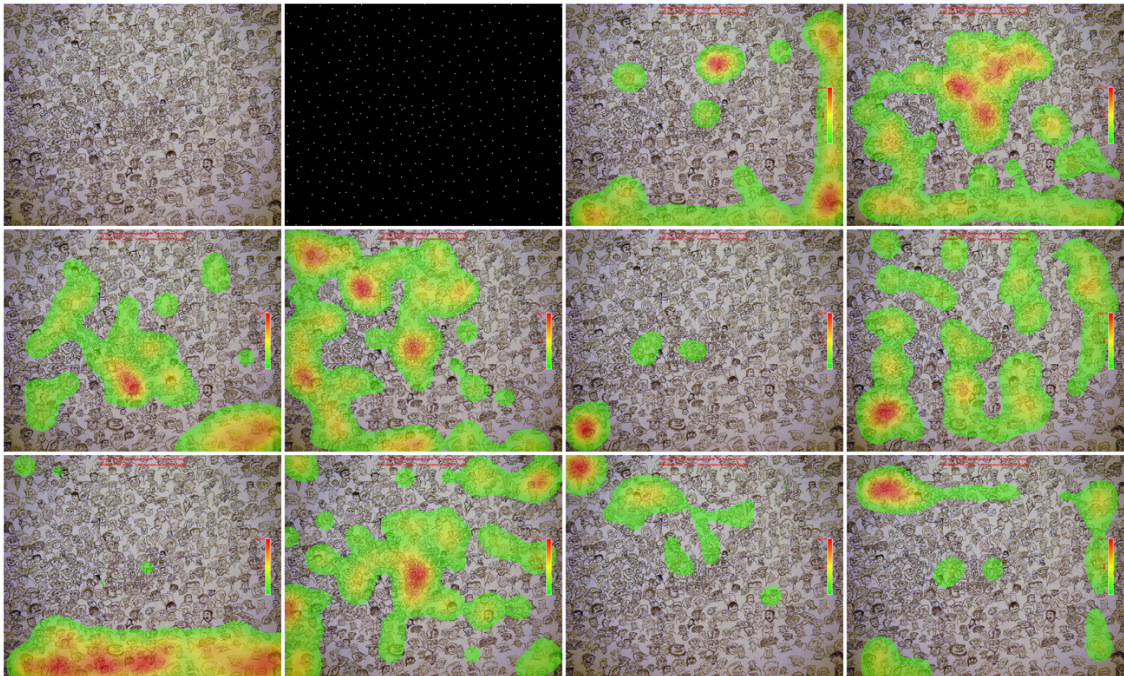


Figure 29: Image grid containing image 22, its annotation and fixation density maps from all subjects.



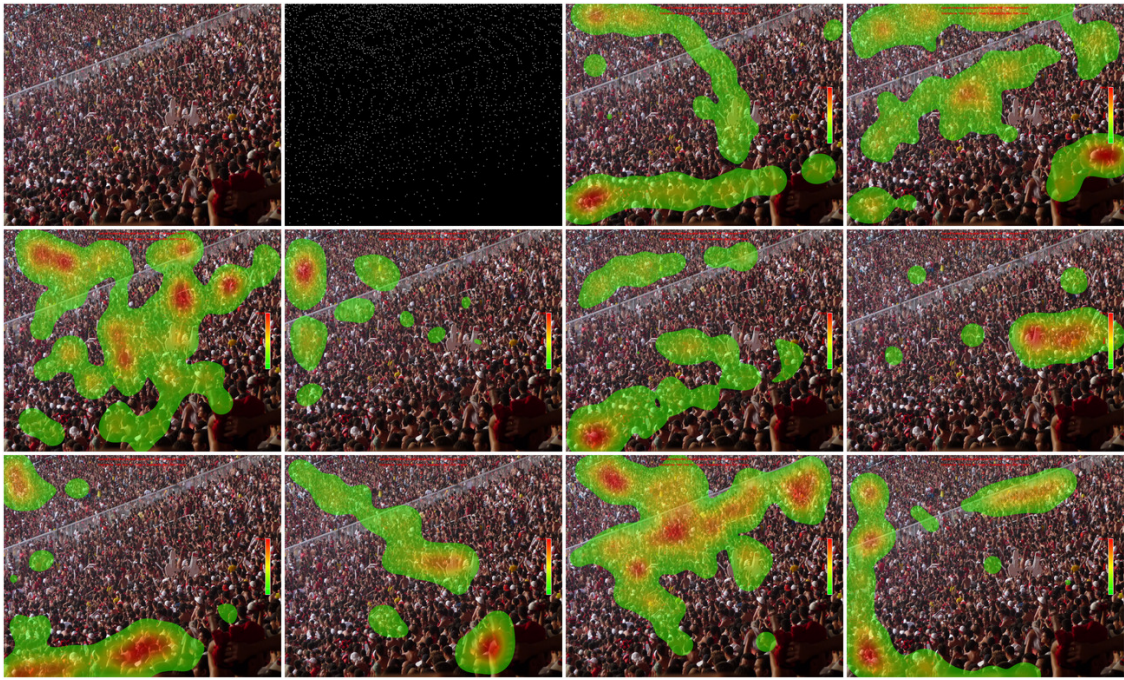


Figure 30: Image grid containing image 23, its annotation and fixation density maps from all subjects.

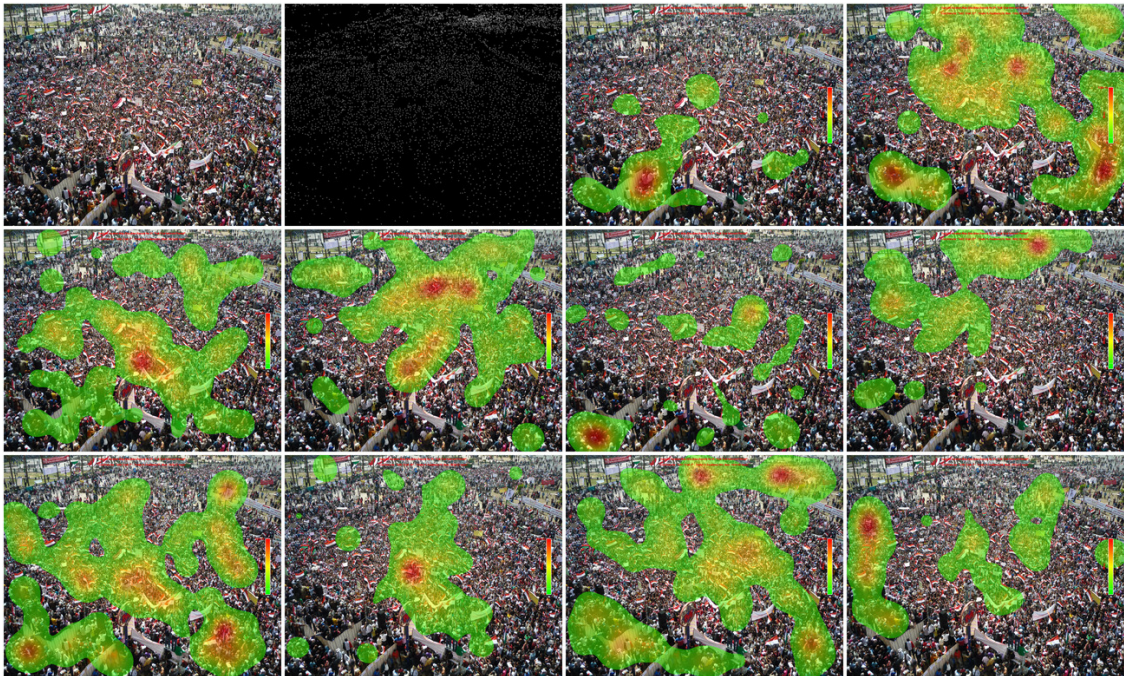


Figure 31: Image grid containing image 24, its annotation and fixation density maps from all subjects.



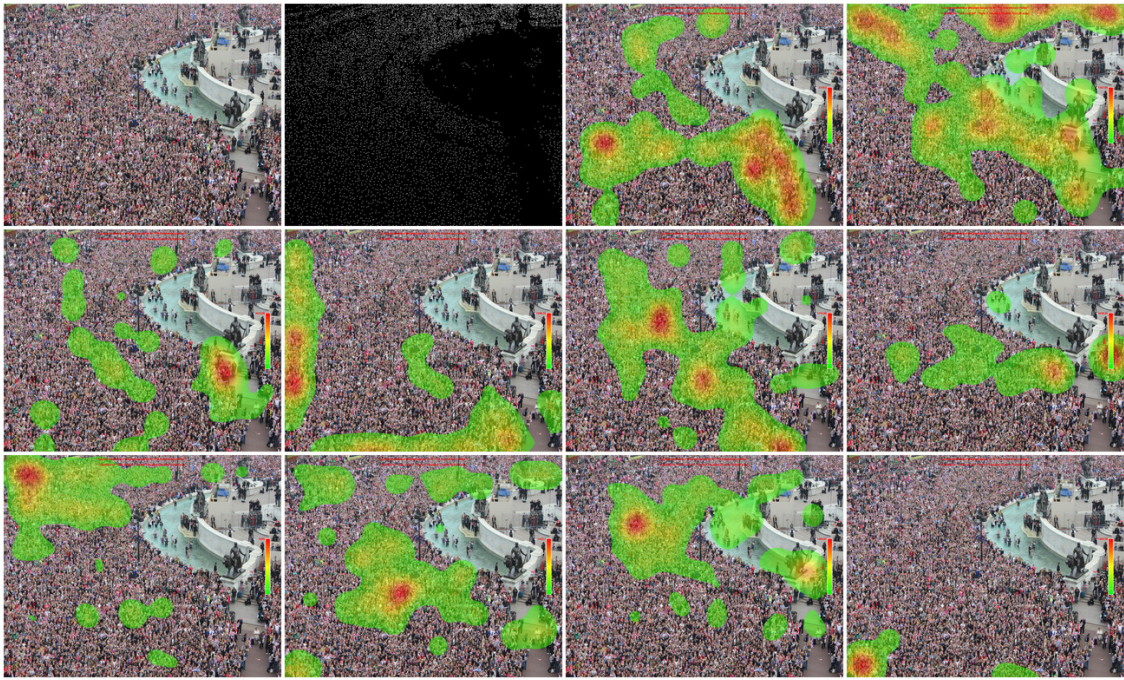


Figure 32: Image grid containing image 25, its annotation and fixation density maps from all subjects.

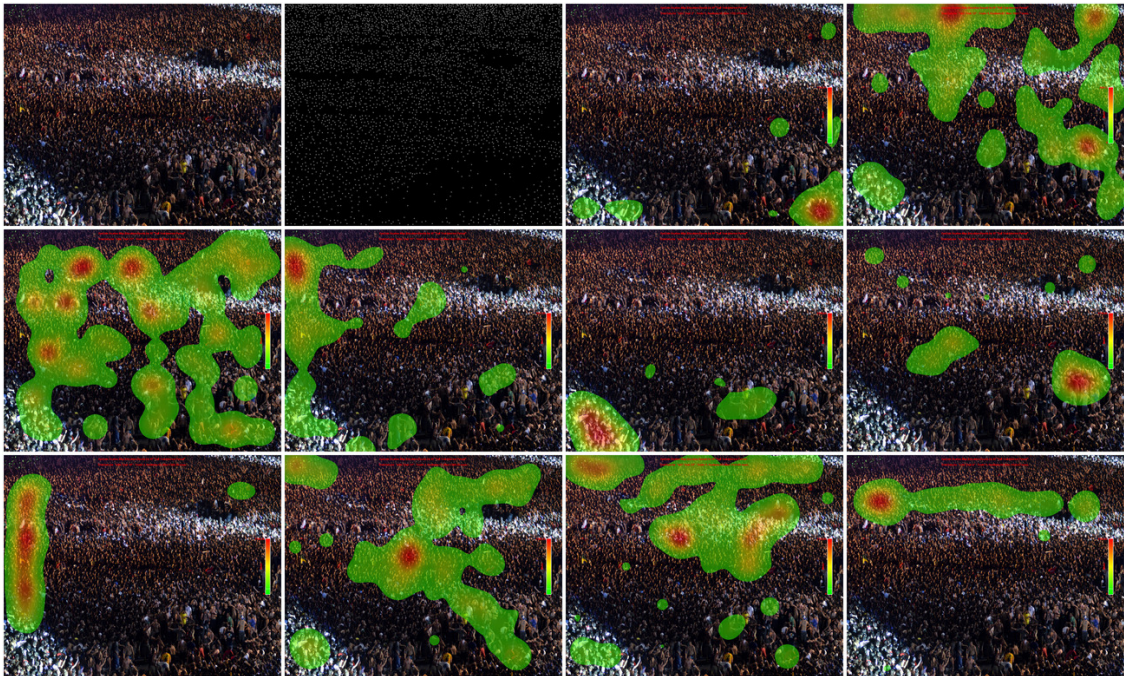


Figure 33: Image grid containing image 26, its annotation and fixation density maps from all subjects.



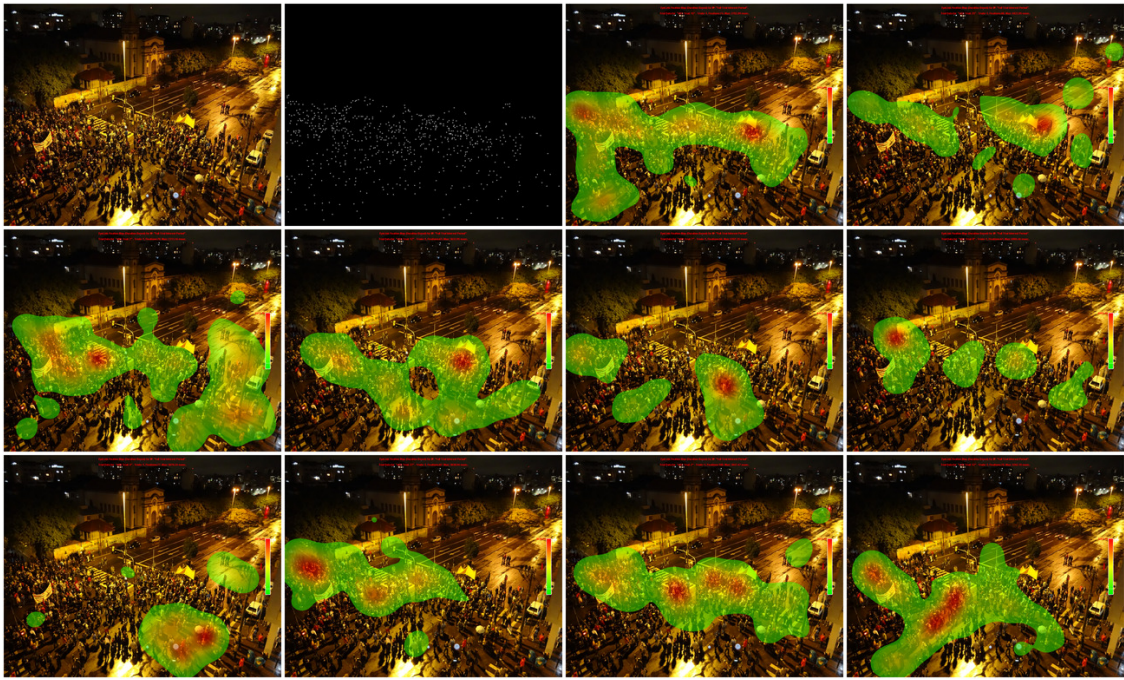


Figure 34: Image grid containing image 27, its annotation and fixation density maps from all subjects.

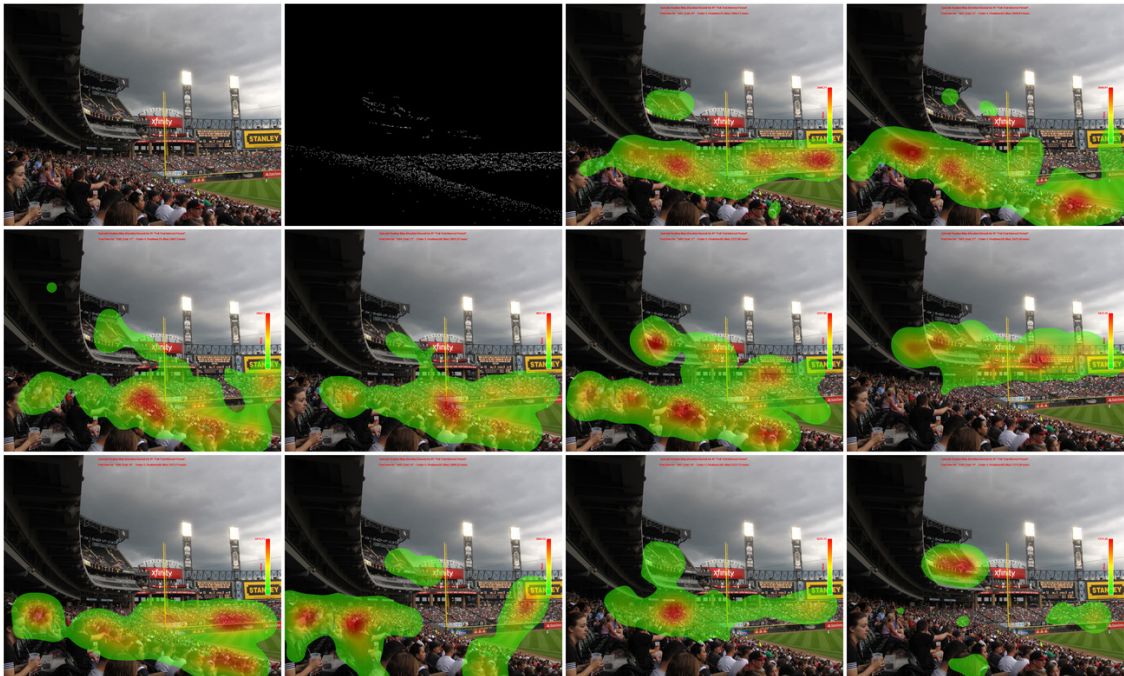


Figure 35: Image grid containing image 28, its annotation and fixation density maps from all subjects.



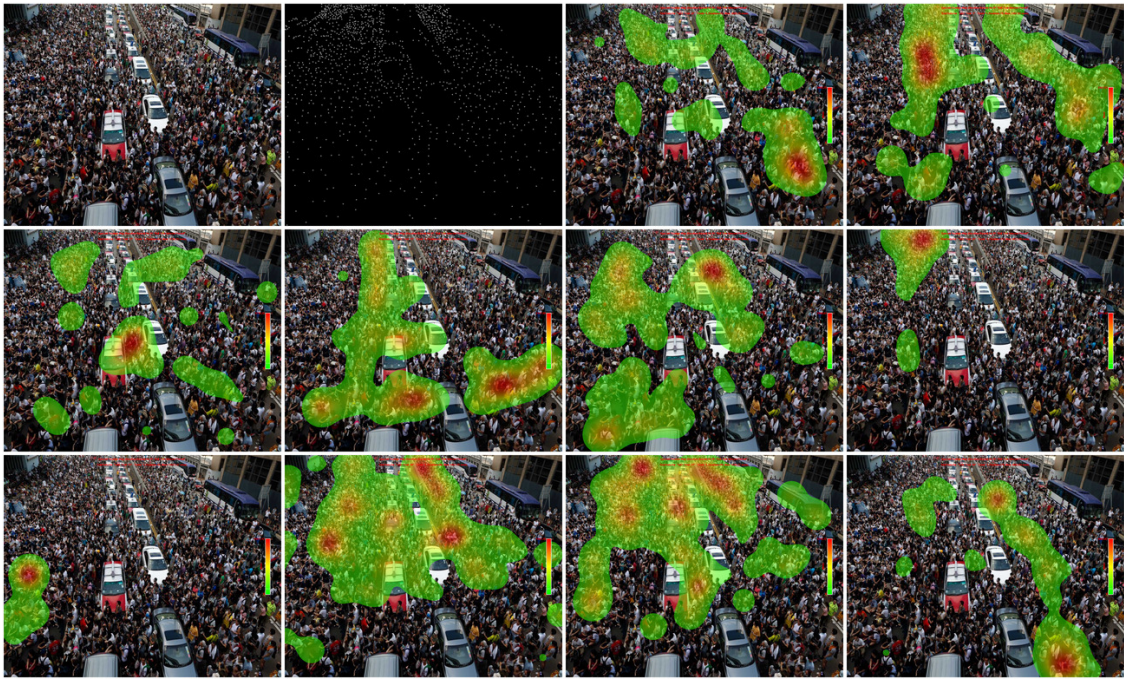


Figure 36: Image grid containing image 29, its annotation and fixation density maps from all subjects.

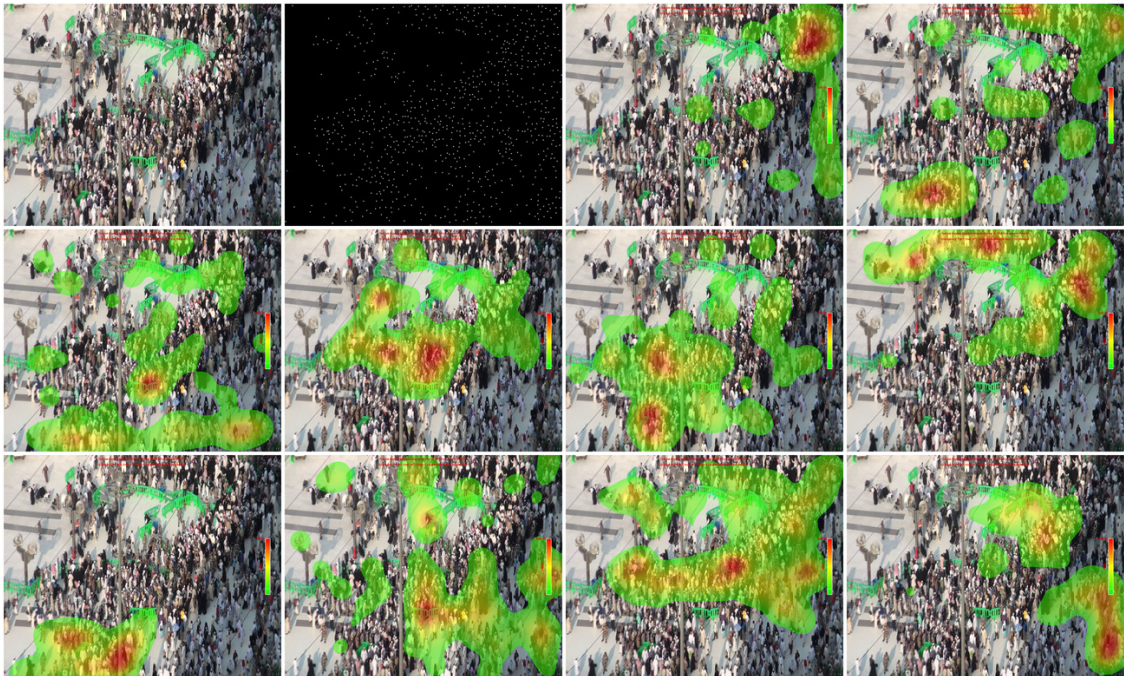


Figure 37: Image grid containing image 30, its annotation and fixation density maps from all subjects.